3-31-2021

Polymer Based Triboelectric Nanogenerator for Cost-Effective Green Energy Generation and Implementation of Surface-Charge Engineering

Diana Lopez

Aminur Rashid Chowdhury
The University of Texas Rio Grande Valley

Abu Masa Abdullah
The University of Texas Rio Grande Valley

Muhtasim Ul Karim Sadaf
The University of Texas Rio Grande Valley

Isaac Martinez
The University of Texas Rio Grande Valley

See next page for additional authors

Recommended Citation

Lopez, D., Chowdhury, A.R., Abdullah, A.M., Sadaf, M.U.K., Martinez, I., Choudhury, B.D., Danti, S., Ellison, C.J., Lozano, K. and Uddin, M.J. (2021), Polymer Based Triboelectric Nanogenerator for Cost-Effective Green Energy Generation and Implementation of Surface-Charge Engineering. Energy Technol., 9: 2001088. https://doi.org/10.1002/ente.202001088

Polymer Based Triboelectric Nanogenerator for Cost-Effective Green Energy Generation and Implementation of Surface-Charge Engineering

Diana Lopez[1], Aminur Rashid Chowdhury[1], Abu Musa Abdullah[1,2], Muhtasim Ul Karim Sadaf[1], Isaac Martinez[1], Brishty Deb Choudhury[1], Serena Danti[3,4], Christopher J. Ellison[5], Karen Lozano[2], M. Jasim Uddin[1]*

[1]Department of Chemistry, Photonics and Energy Research Laboratory, University of Texas Rio Grande Valley, 1201 W. University Drive, Edinburg, Texas, 78539, USA

[2]Department of Mechanical Engineering, University of Texas Rio Grande Valley, 1201 W. University Drive, Edinburg, Texas, 78539, USA

[3]Department of Civil and Industrial Engineering, University of Pisa, Largo L. Lazzarino 2, 56122 Pisa, Italy

[4]Department of Civil and Environmental Engineering, Massachusetts Institute of Technology, Cambridge, MA 02142, USA

[5]Dept. of Chemical Engineering and Materials Science, The University of Minnesota, 421 Washington Ave SE, Minneapolis, MN 55455

*Corresponding author email: mohammed.uddin@utrgv.edu,

Abstract: Performance of triboelectric nanogenerators for harvesting mechanical energy from the ambient environment has been limited by structural complexity, cost-effectiveness, and mechanical weakness of materials. Here, we report on a cost-effective vertical contact separation mode triboelectric nanogenerator using PE and PC in a regular digital versatile disc. This cost-effective nanogenerator with simplified structures was able to generate an open circuit voltage of 215.3 V and short circuit current of 80 µA. The effects of the distance of impact and the air gap between the triboelectric layers have also been tested from 3 to 9 cm, and 0.25 to 1 cm, respectively. It was determined that 0.5 cm was the optimal air gap. The nanogenerator was also tested in different real-life scenarios including stresses produced by a moving car, walking, and a rolling skateboard over the nanogenerator. The surfaces of the triboelectric layers were further modified by surface-charge

This article has been accepted for publication and undergone full peer review but has not been through the copyediting, typesetting, pagination and proofreading process, which may lead to differences between this version and the Version of Record. Please cite this article as doi: 10.1002/ente.202001088.

engineering which induced a 460% increase in the output power. These tests revealed a significant electrical response and mechanical stability under stress. In summary, this study demonstrated that the relatively inexpensive PE and PC triboelectric pair has the potential to be used for highly efficient, mechanically robust triboelectric nanogenerators.

Introduction:

Due to the increasing depletion of fossil fuels, scientists have been searching for renewable and environmentally friendly power sources [1,2]. Traditional power supplies, such as batteries used in electronics, have a limited lifetime and are usually composed of expensive and environmentally hazardous components [3]. To avoid these issues and provide a more sustainable power source, scientists have long been trying to use the abundant amount of ambient waste mechanical energy to generate electricity [2,4]. This includes raindrops, human footfalls, and ocean waves, among others [5]. There are several material-based strategies that can convert mechanical energy into electricity including exploitation of piezoelectric, electromagnetic, or electrostatic effects. Using such material properties to obtain clean energy is possible; however, several limitations have prevented their application on a large scale, including structural complexity, difficulty of large-scale fabrication of high-quality materials, and dependence on external power sources. In addition, efficient energy harvesting can be limited to a very narrow range of applied frequencies [6,7]. As most environmental mechanical energy sources have a wide range of natural frequencies, these techniques for harvesting energy become ineffective in many cases. [8]. Recently, a new type of power generating device, called a triboelectric nanogenerator (TENG), has been attracting increasing attention; this device utilizes both triboelectric and electrostatic effects, which at the nanometer scale, convert mechanical energy into electrical energy [910]. The TENG's working principle is based on the Maxwell's displacement current, where the term related to polarization-induced current $\frac{\partial P}{\partial t}$ is directly correlated to the output current [6]. The polarization-induced current is generated due to the combined effect of triboelectrification and electrostatic induction; when two surfaces with different

polarities come into contact, an electron transfer occurs across the interface to make up the potential difference between the surfaces. This charge separation leads to the conversion of mechanical energy into electrical energy. TENG devices can operate in a broad range of vibrational frequencies instead of a single resonant frequency. Moreover, they can respond to low frequency vibrations, namely, in the range where most environmental vibrations exist, such as wind energy [11,12], vehicle movement [13], tree leaf movement [14], human walking [15], etc. A typical TENG device can be implemented by carefully assembling two electrodes made from triboelectrically active materials. When mechanical energy is applied, the device capacitance changes (due to a change in displacement), which leads to a flow of current between the two conductive electrodes and associated power generation [16]. The current in the TENG flows back and forth between the electrodes in an alternating current mode [17]. Intuitively, the performance of a TENG device can be controlled by tuning the charge density on the triboelectric surface. TENG devices can adapt well to various mechanical energy types by different modes of operation such as vertical contact-separation, lateral sliding, single electrode, and freestanding modes [18,19]. The potential applications include sensors [20], environmental monitoring, medical devices [20], personal electronics, and defense technology [21]. TENG devices have demonstrated instantaneous conversion efficiency of 70% and a total energy conversion efficiency of up to 85% [22].

There have been several attempts to fabricate highly efficient TENGs, mainly focusing on the use of expensive materials [22–24]. At the same time, other studies have investigated TENGs with readily available, cost-effective materials [25,26]. However, to date, these cost-effective materials have produced relatively low performance in terms of power production. In this study, we present a TENG based on a vertical contact separation mode using polyethylene (PE) and polycarbonate (PC). PE and PC were used to create a TENG to power small devices using vibrational energy available from various transportation sources. The materials are readily available in the market and require no special preparation or synthesis which provides us with the opportunity to produce very low cost TENGs. In our study, we tested the open circuit voltage and short circuit current of the

TENG under different load conditions and frequencies. We also measured the rectified response of the TENG using a bridge rectifier. The charging capacity of the TENG was tested with 1, 3.3, and 4.7 μF capacitors. The practical application of the TENG was illustrated by measuring the TENG output during human walking, skateboard riding, and truck moving over the TENG. Furthermore, enhancement of the TENG performance was obtained by incorporating an inexpensive surface-charge engineering method [27].

Results and Discussion:

We successfully fabricated a polymer-based TENG, composed of PC and PE layers connected through copper electrodes; PC and PE layers were separated by three 2mm x 5mm x 1mm sized Polyurethane (PU) foams. PU foam has been widely used as a spacer in triboelectric nanogenerators [6,15,28]. The nanogenerator was tested at different load frequencies as well as in real life scenarios.

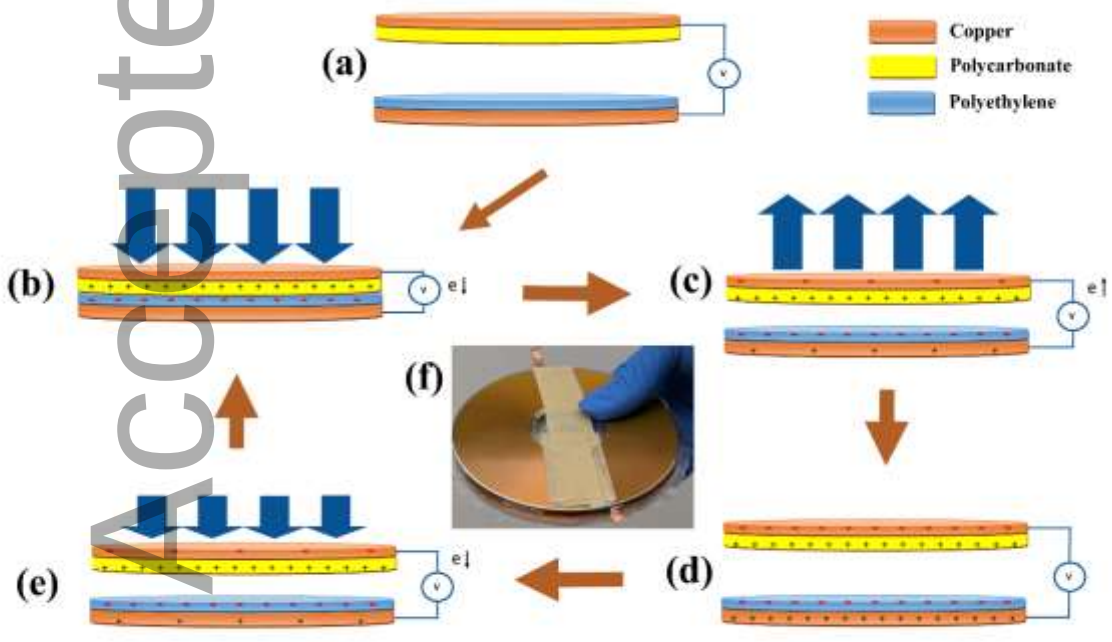

Figure 1: Working mechanism of the polymer-based TENG: (a) initial stage of the device, (b) both layers in full contact in the presence of an external force, (c) separation begins due to the release of

the external force, (d) the device in full separation mode and (e) application of the external force on the device again. (f) Optical image of the TENG.

Figure 1 shows the working mechanism of the polymer-based TENG. PU spacers have not been shown in the figure for simplicity of the mechanism. At the initial stage (Figure 1(a)), the upper PC layer and the lower PE layer are kept at 0.5 cm. According to the triboelectric series, the PC surface will donate electrons to the PE surface [29,30]. The lower surface of the PE layer gains electrons and becomes negatively charged in the initial position. When an external force is applied on the device, the layers establish contact with each other (Figure 1(b)). As the external force is removed from the device, both surfaces begin separating and the upper layer moves upward, which induces a higher electrical potential at the lower electrode (Figure 1(c)) [23,30]. To balance the effect of triboelectrification and electrostatic induction, electrons move from the electrode of the lower part to the upper part [22,30,31]. The electrons stop moving after the device is fully separated (Figure 1(d)) [23]. As the external force is then reapplied, and the upper PC layer starts moving towards the lower PE layer. At this stage, the electrons will start moving from the upper electrode towards the lower one due to the higher potential of the upper electrode. The electrons flow until the device establishes full contact mode. FTIR characterization of polyethylene and polycarbonate has been shown on Supplementary Figure S2. All the characteristic bands for the polycarbonate and polyethylene are present in the FTIR spectra and they are tabulated in the Supplementary Table 1 and 2 respectively [32–34].

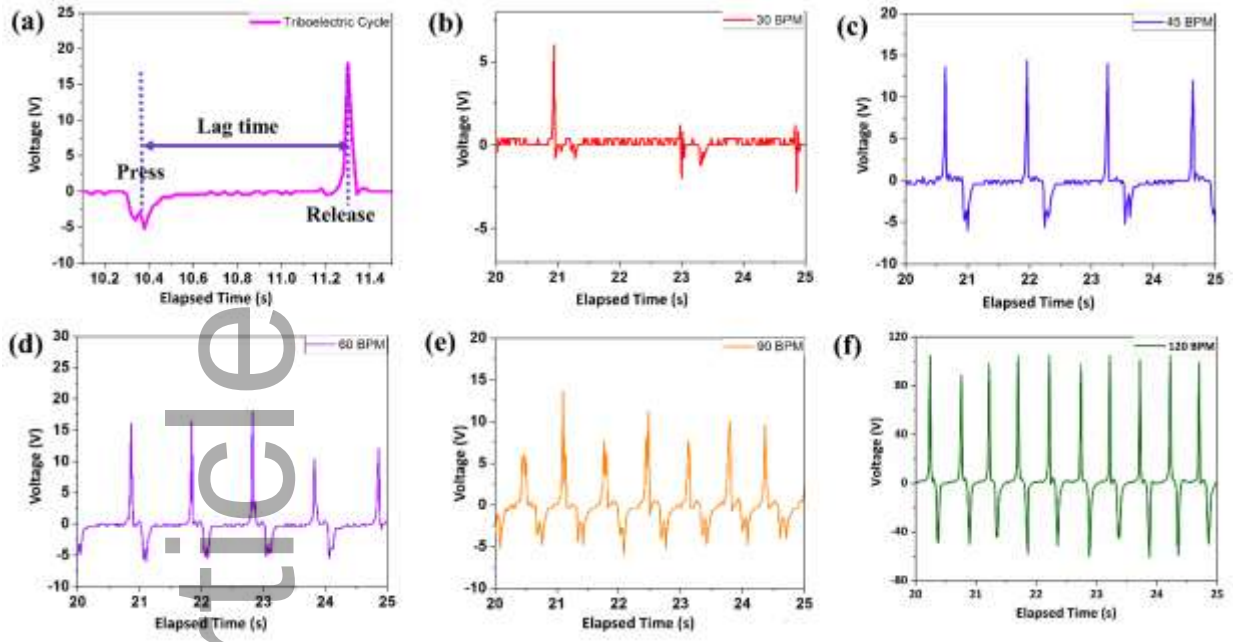

Figure 2: (a) Typical contact and release voltage response of the TENG. Representative open-circuit voltage response of the nanogenerator under different load frequencies at (b) 30 BPM, (c) 45 BPM, (d) 60 BPM, (e) 90 BPM and (f) 120 BPM.

To demonstrate the operation of the nanogenerator, it was tested under different conditions. First, the nanogenerator was tested at different frequencies (described as beats per minute; BPM) of hand tapping. The TENG was tested at 30 BPM, 45 BPM, 60 BPM, 90 BPM, and 120 BPM. Figure 2 demonstrates the TENG output potential in the triboelectric cycle. Figure 2(a) shows two distinct depressions and peaks due to contact and release of the TENG. The TENG shows a negative (depression) peak due to slower contact. As the nanogenerator is relatively large compared to the area of the part of the hand that contacts it while tapping, the deformation due to the tapping and the contact resulting from it is not uniform. Figures 2(b)-(f) show the voltage responses for multiple contact and release cycles. This can be easily explained by understanding that a little nonuniform applied load may cause zonal contact. This will make a local depression or peak (depending on the polarity of electrical connection). As the mechanical load is repetitively applied, the triboelectric parts come into contact, and after the contact, they start moving apart due to the reflex of the PU spacer. This results in partial diminution of signals due to the proximity of the triboelectric layers

on the opposite sections. The fluctuation in the signal in Figure 2(a) between 10.3 s and 10.4 s is related to this asynchrony effect. Diminution of signals and fluctuation is visible in Figure 2(b) to Figure 2(f). The sharp peak in Figure 2(a) results from the release of applied stress in the TENG. As soon as the stress is released, the entire TENG experiences a sudden reflex from the PU foam which releases all the energy and rapidly returns to its original position. In addition, the fluctuation in the voltage and sudden rise can be attributed to human error as the outputs were generated by finger tapping motion.

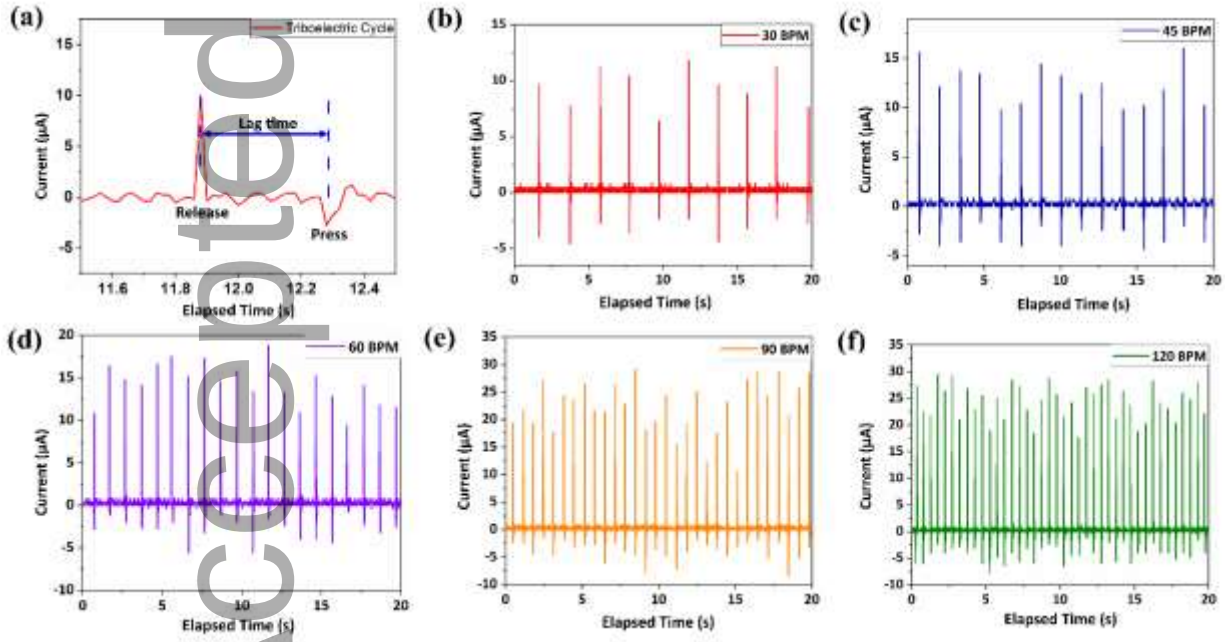

Figure 3: Representative current response of the nanogenerator under different load frequencies at (b) 30 BPM, (c) 45 BPM, (d) 60 BPM, (e) 90 BPM, and (f) 120 BPM.

Figure 3 shows the generation and transfer of charge from the triboelectric nanogenerator to the circuit. As soon as the TENG faces external stresses, which bring the triboelectric layers closer together, the triboelectricity starts its action. As they approach each other, the negative layer (i.e.,

PE) accumulates negative charge on its surface and the positive layer (i.e., PC) does the opposite. As they move apart, the triboelectric layers generate exactly the opposite charge flow owing to opposite charge generation in the triboelectric layers. As the generation of triboelectricity is dependent on contact-separation mode, the TENG shows an opposite peak when the triboelectric layers are returning to their initial position where they are fully separated. These opposite peaks (i.e. release and stress) are shown in Figure 3(a). Under applied stress, TENG triboelectric layers slowly reach each other in comparison to the return to their initial state of full separation. This slower action generates a smaller peak due to smaller charge transfer density from one surface to another surface over a relatively larger contact time. However, at the moment of stress release, the TENG immediately returns to its original position. This immediate return generates a sudden charge transfer from one surface to another surface through the circuit connected to the electrodes. Figure 3(b-f) shows the electricity generation response by the TENG under different tapping frequencies. It has been observed that the current production increases with the increase of tapping frequency. The average short-circuit current outputs were 9.44, 12.29, 14.21, 22.1 and, 24.32 μA for 30, 45, 60, 90, and 120 BPM load frequencies respectively. During the tapping motion, the impact velocity increases with the increase of tapping frequency. And this increase in tapping frequency leaves the electrons with a shorter time to neutralize the charge and that results in a higher flow of electrons [26,35,36].

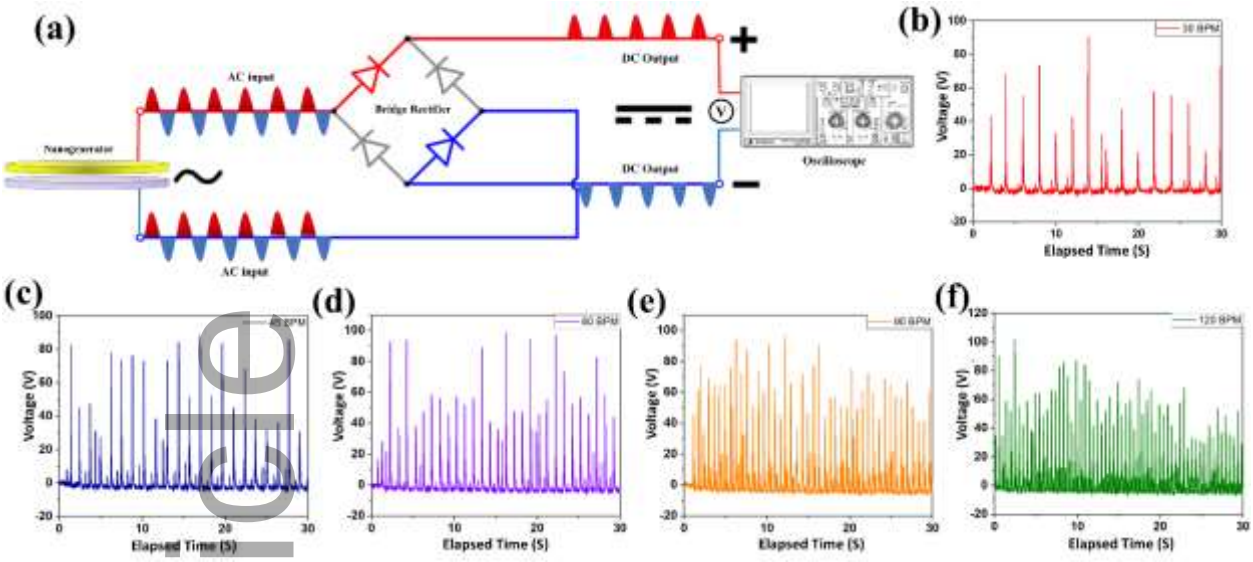

Figure 4: Rectified output voltage of TENG: (a) schematic representation of circuitry connection to oscilloscope with bridge rectifier. Output voltage of TENG at load frequencies of (b) 30 BPM, (c) 45 BPM, (d) 60 BPM, (e) 90 BPM, and (f) 120 BPM.

The rectified response of the nanogenerator at different BPM is shown in Figures 2 and 3. The recorded voltage and current are due to contact and release of the two triboelectric layers (PE and PC) as described earlier. The rectified voltage signal in Figure 4 is a representation of the open-circuit voltage achieved at different frequencies. The output voltage reached over 102.4 V with an average ranging between 60V to 80V in variable BPM configuration. Figure 4(a) demonstrates the circuitry connection used in measurement of the potential. From Figures 2(b)-(d) we can see inconsistent amplitude of the voltage with the applied load. The output voltage depends on the application of the external force and frequency [37]. But due to the uneven application of the load during the experiment, resulting from human error, here we can see variable voltage amplitude. This demonstrates the ability of the TENG to produce a relatively constant voltage depending on the application of the force. Peak voltage increases from 30 BPM (Figure 2(b)) to 45 BPM (Figure 2(c)). However, it is noticeable that the density of peak voltage with more than 80 V from Figure 4(c) to Figure 4(f) is decreased. As the number of contacts between the PE and PC surfaces increases, the charge production increases. In a similar way, the transfer of the negative charge

accumulated in the PE layer occurs rapidly throughout the circuit due to the proximity of the aluminum layer next to PE and PC. This transfer of charge is also a consequence of the higher number of charges accumulated in the opposite surfaces of the triboelectric layer during the reciprocating action. Owing to the low conductivity of PE and PC, a fraction of the charge generated in every stress-release cycle remains in the triboelectric layers of the TENG, which conveys the potential and the charge change from cycle to cycle.

Rectified current output of the TENG in various load frequencies is shown in Supplementary Figure S1. In this case, the amplitude of current produced is gradually increasing from 8-10 µA to 25-26 µA. However, there is a noticeable (2-3 µA) decrease in the current production from 45 BPM to 60 BPM. This is due to an increase in charge generation for higher contact and release frequency. The conductive layers are not able to extract most of the charge and pass it through the circuits. This makes the flow of electrons less than expected, which shows as a decrease in current. Higher current generation numbers are due to the higher number of contacts and releases, which in turn makes higher charge generation following by flow of charge through a closed circuit.

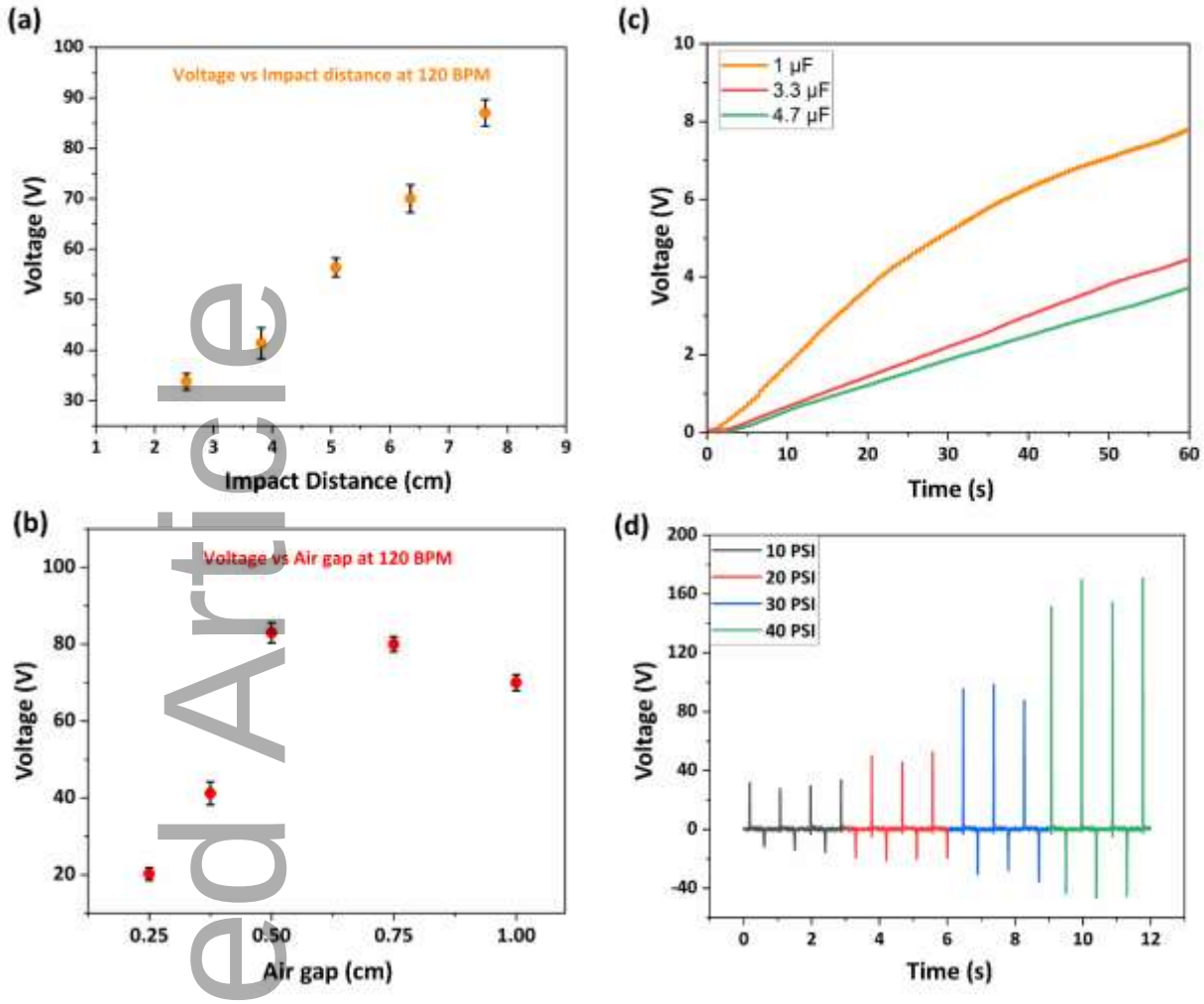

Figure 5: Observed voltage for variable (a) tapping distance, (b) triboelectric air gap. (c) Charging capacitors of variable capacitance for 60 seconds at 120 BPM. (d) Voltage output at variable pressure.

Figure 5(a) shows the change in triboelectric open circuit voltage in response to the variable impact distance that is measured from the range of hand movements during triboelectric tapping. The output performance of the device was tested for variable impact distance. The distance of impact ranged between 3 and 8 cm; the impact was tapping, and it was conducted at 120 BPM. Figure 5(a) shows that as the impact distance increased, the voltage increased linearly from 33.8 V to 87 V. As the impact distance increases, the force due to the impact on the triboelectric surface also increases directly. Since the frequency of tapping is kept constant, the velocity of the finger increases with increased impact distance [37]. Hence, the momentum increases with the increased velocity, leading

towards higher force of impact. This magnified force leads to larger deformation of the contact surface of the triboelectric layers, resulting in higher output voltage[37].

Figure 5(b) shows that the open circuit voltage increases with the increase of air gap and reaches a maximum value when the air gap is around 10 times the thickness of the materials [38]. In our study that maximum gap was 0.5 cm and after that there was no significant increase in voltage, while the structural integrity of the device was becoming compromised as the gap increased further. Considering all these factors, we chose 0.5 cm as the optimal air gap.

Figure 5(c) shows the charging capacity of the nanogenerator at various capacitances. Capacitors of 1, 3.3, and 4.7 μF were used for the test at 120 BPM. Figure 5(c) shows the open circuit voltage for charging the capacitor for 60 s at 120 BPM. With increasing capacitance, the rate charging declined. By using a full wave bridge rectifier made with 4 diodes, the device was able to power the 1, 3.3, and 4.7 μF capacitors to 3.68, 4.43 and 7.76 V in 60 seconds at 120 BPM, respectively. Here, the low charging voltage of capacitors is related to the electrical energy loss in the full wave bridge rectifier[39].

Figure 5(d) shows the response of the nanogenerator at variable pressures. The test was conducted at 75 BPM load frequency with pressures varying in the range of 10 to 40 PSI. A pneumatic piston of 2 cm in diameter applied the pressure on the device. As the pressure increases, the force also increases, and the value of force can be found by multiplying the cross-sectional area of the piston with the corresponding pressure. The maximum voltage output was observed to be 170.6V for 40 PSI. It can be clearly seen that the output increases with the increase of pressure and the output signals have a uniform response when subjected to a specific pressure. This suggests that the nanogenerator can be implemented as a force sensor. Supplementary Figure S3 shows the average output voltage of the nanogenerator for 10 to 40 PSI pressure with error bars signifying the standard deviation for each of the values. And from supplementary figure S3, it is observed that the output voltage increases non-linearly as a function of pressure.

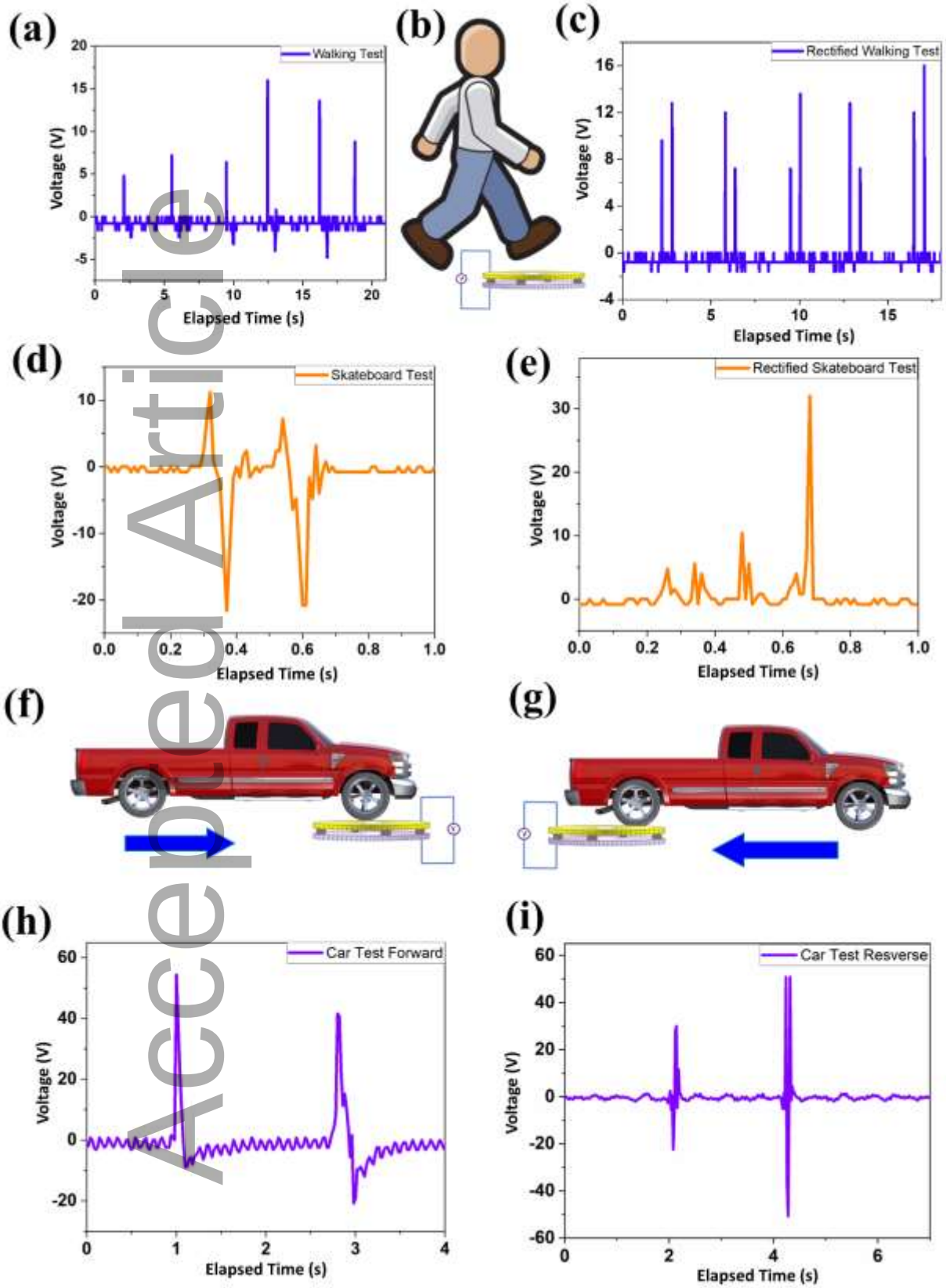

Figure 6: Testing TENG in daily traffic conditions: (a) electrical voltage output in (b) human walking (schematic view), (c) rectified response of triboelectric nanogenerator in human walking;

(d) Regular response and (e) rectified response of nanogenerator under skateboard movement; schematic representation of (f) forward and (g) backward movement of truck over triboelectric nanogenerator. Open-circuit voltage response of truck test on nanogenerator under (h) forward and (i) backward motion.

The TENG was tested in different real-life conditions, from regular to extreme, to prove its potential of usability in pavement or road. The nanogenerator showed an impressive response with extreme mechanical stability under different load conditions. Figure 6 demonstrates the response of the nanogenerator under different load conditions. The TENG was tested with regular walking of a human subject. For this purpose, the TENG was placed on a regular walkway while the subject was asked to walk at a regular pace. TENG response was found to produce promising values up to 20 V. Figure 6(a, c) highlights the response (i.e., regular and rectified) of an average build person walking on the nanogenerator. The signal demonstrates a relatively smaller peak followed by a larger peak. The smaller peak is related to slower step on the TENG followed by the movement of the triboelectric PE and PC towards each other. The large peak followed by a smaller peak is related to the sudden release of the step from the nanogenerator. This is larger (30 V) than the step-on peak due to faster movement of the TENG during walking out. The TENG was also tested with a rolling skateboard carrying a human subject. In this condition, the TENG showed a distinct peak (peak-to-peak voltage 30 V) during the skateboard testing. The peak is complex in shape compared to the response of walking due to the multiple impacts and releases by the four wheels of the skateboard rolling on the nanogenerator. During skateboard testing, the TENG is initially impacted by the two front wheels, causing a sharp rise in voltage. As the skateboard moves forward, the points of wheel impact change. Simultaneously, the wheels on the back of the skateboard start rolling over the TENG and there the triboelectric layers come closer, while farther ahead the layers are moving away. In Figure 5(e), the TENG rectified response of skateboard displays increasing response with repetitive stresses and releases. The skateboard test showed a highest response of 35 V during the test which is larger than that of the walking test. By comparing both tests, it can be highlighted that

the TENG shows a higher potential with faster stress impact. Therefore, the TENG was tested with the highest amount of stress available in everyday road/pavement conditions by moving a pickup truck, weighing 5300 lbs, over the nanogenerator. In these conditions, the TENG showed two distinct peaks represented in Figure 6(h, i) as a response of moving forward and backward. While the truck moves forward the nanogenerator is stressed by the front wheels, which bear most of the truck's weight, followed by the back wheels supporting lighter parts. Heavier parts in front generated larger peaks because of higher load while the lighter load on the back wheels generated smaller potentials. Rough fluctuation in peak is governed by gradual movement of the wheel from front to back.

To enhance the performance of the TENG, surface-charge engineering was implemented. We performed physical sliding on the PE layer with aluminum. For this treatment, PE was rinsed with anhydrous ethanol and then it was dried in the ambient air for a duration of 24 hours; this led to the minimization of possible existing surface charges. After that the PE layer was physically slid with aluminum for 100 cycles to ensure equilibrium of charge transfer [40]. This treatment pre-loaded the PE layer with a substantial amount of extra surface charge and resulted in higher output. This kind of surface modification has been found to be practically stable [27].

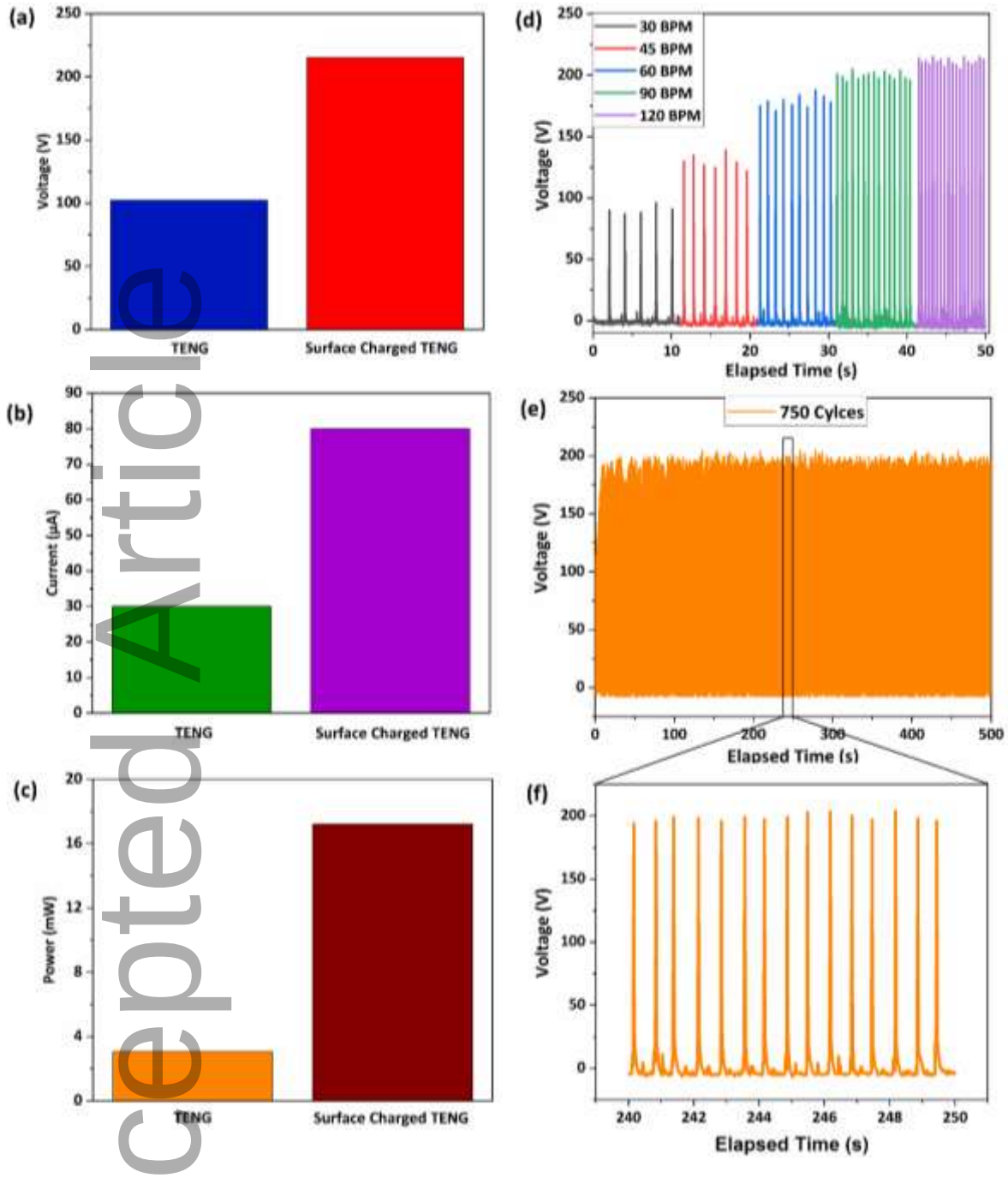

Figure 7: Side by side comparison of (a) maximum rectified output voltage, (b) maximum rectified current, (c) maximum rectified power output at 120 BPM, (d) Rectified output voltage of TENG for different frequencies, (e) Rectified voltage response of TENG during 750 load cycles, (f) Enlarged view of the TENG response during load cycles.

The surface charged TENG was tested at 120 BPM while maintaining the 0.5 cm air gap. Figure 7(a) shows that the maximum rectified output voltage with the surface charged TENG was found to be 215.3 V, which was a 110% increase in output voltage. Similarly, with current, we saw an

increase of 50 μA as evident by Figure 7(b). Figure 7(c) shows that the output power increased by 14.128 mw. The voltage response at varying tapping frequencies was also measured and it was observed that there was an increase in output with the increment of the BPM indicating that the surface charge engineering has induces stability onto the TENG; the stability is further shown in Figure 7(e) where the TENG shows rectified output voltage for 750 cycles at 90 BPM. Figure 7 (e) shows a stable voltage output throughout the entire cycle indicating a good stability of the device.

Conclusion:

In summary, we have successfully demonstrated that the vertical contact-separation polymer-based TENG can dramatically achieve high potential output. The key factors that enable the TENG to have a high output response consist of its simplified structure and large surface contact area. The simplified design of the TENG consisted of common materials available in our daily lives such as polycarbonate and polyethylene, with polyurethane spacers and copper electrodes. The triboelectric nanogenerator was first tested with the external force of human footsteps at different BPMs. The TENG was found to have a high rectified voltage of over 100 V and a short-circuit current of approximately 25 μA which further increased to 215.3 V and 80 μA after surface-charge engineering. Furthermore, due to its great performance under external force of human footsteps, it was decided to test the TENG with more extreme applications, namely, skateboard riding and truck driving. With each application tested, an increase in voltage is shown, thus demonstrating that with further surface contact the two materials produce higher potential energy. Human walking showed a high rectified output of over 16 V. The second application of the skateboard test showed an increase to over 30 V. The final application the truck demonstrated the highest output of over 50 V. It can be concluded that these daily life conditions can be very successful in achieving high potential output that can be harvested into electrical energy. The observations made in this research should pave the

way to study and improve the use of these materials. This TENG reveals the ability of polymer-based TENGs for potential use in large scale applications, such as roads, sidewalks, or flooring that can produce electrical energy in a step toward the greater use of green power sources.

Acknowledgement:

This research was supported by the National Science Foundation (NSF PREM) award under grant No. DMR-1523577: UTRGV-UMN Partnership for Fostering Innovation by Bridging Excellence in Research and Student Success. This project was partially supported by the Welch Foundation Award: BX-0048.

Experimental Methods:

Preparation of Triboelectric Nanogenerator: The triboelectric nanogenerator was prepared using commercial Digital Versatile Disc as mechanical support for negative Polyethylene layer. This PE layer was attached to the disc using a heat wave of air. Polycarbonate on DVD worked as the positive layer of the triboelectric nanogenerator. The aluminum layer inside the DVD worked as the charge collecting portion. Copper tapes were connected to both aluminum layers which were used as electrodes to measure the signal output. Three 2mm x 5mm x 1mm sized PU foams were placed equidistantly on the edge of the discs.

Preparation of Bridge Rectifier: The bridge rectifier is made with rectifier diode comprising of 1N5399 type four diode added as shown in figure 2 and figure 4.

Output Measurement:

Electrical contacts were made by attaching wires to the two copper tapes connected to two electrodes of Tektronix TDS 1001B. Single channel connections were used to ensure minimal inteference.

FTIR Characterization:

Fourier-transform Infrared Spectroscopic analysis was performed using a VERTEX 70v FTIR Spectrometer. Relative transmittance was collected in transmittance mode over a full range of 4000-450 cm^{-1} wavenumber. FTIR characterization is shown in Supplementary Figure S2.

References:

(1) Eaton, E. M.; Day, N. A. Petro-Pedagogy: Fossil Fuel Interests and the Obstruction of Climate Justice in Public Education. *Environ. Educ. Res.* **2019**, *0* (0), 1–17. https://doi.org/10.1080/13504622.2019.1650164.

(2) Hussain, I.; Tran, H. P.; Jaksik, J.; Moore, J.; Islam, N.; Uddin, M. J. Functional Materials, Device Architecture, and Flexibility of Perovskite Solar Cell. *Emergent Mater.* **2018**. https://doi.org/10.1007/s42247-018-0013-1.

(3) Weng, B.; Xu, F.; Alcoutlabi, M.; Mao, Y.; Lozano, K. Fibrous Cellulose Membrane Mass Produced via Forcespinning® for Lithium-Ion Battery Separators. *Cellulose* **2015**, *22* (2), 1311–1320. https://doi.org/10.1007/s10570-015-0564-8.

(4) Hussain, I.; Chowdhury, A. R.; Jaksik, J.; Grissom, G.; Touhami, A.; Ibrahim, E. E.; Schauer, M.; Okoli, O.; Uddin, M. J. Conductive Glass Free Carbon Nanotube Micro Yarn Based Perovskite Solar Cells. *Appl. Surf. Sci.* **2019**, *478*, 327–333. https://doi.org/10.1016/j.apsusc.2019.01.233.

(5) Zhu, G.; Lin, Z.-H.; Jing, Q.; Bai, P.; Pan, C.; Yang, Y.; Zhou, Y.; Wang, Z. L. Toward Large-Scale Energy Harvesting by a Nanoparticle-Enhanced Triboelectric Nanogenerator. *Nano Lett.* **2013**, *13* (2), 847–853. https://doi.org/10.1021/nl4001053.

(6) Chen, J.; Wang, Z. L. Reviving Vibration Energy Harvesting and Self-Powered Sensing by a Triboelectric Nanogenerator. *Joule* **2017**, *1* (3), 480–521. https://doi.org/10.1016/j.joule.2017.09.004.

(7) Park, J. Y.; Salauddin, M.; Rasel, M. S. Nanogenerator for Scavenging Low Frequency Vibrations. *J. Micromechanics Microengineering* **2019**, *29* (5), 053001. https://doi.org/10.1088/1361-6439/ab0241.

(8) Chen, J.; Zhu, G.; Yang, W.; Jing, Q.; Bai, P.; Yang, Y.; Hou, T.-C.; Wang, Z. L. Harmonic-Resonator-Based Triboelectric Nanogenerator as a Sustainable Power Source and a Self-Powered Active Vibration Sensor. *Adv. Mater.* **2013**, *25* (42), 6094–6099. https://doi.org/10.1002/adma.201302397.

(9) Lee, K. Y.; Chun, J.; Lee, J.-H.; Kim, K. N.; Kang, N.-R.; Kim, J.-Y.; Kim, M. H.; Shin, K.-S.; Gupta, M. K.; Baik, J. M.; Kim, S.-W. Hydrophobic Sponge Structure-Based Triboelectric Nanogenerator. *Adv. Mater.* **2014**, *26* (29), 5037–5042. https://doi.org/10.1002/adma.201401184.

(10) Yang, Y.; Lin, L.; Zhang, Y.; Jing, Q.; Hou, T.-C.; Wang, Z. L. Self-Powered Magnetic Sensor Based on a Triboelectric Nanogenerator. *ACS Nano* **2012**, *6* (11), 10378–10383. https://doi.org/10.1021/nn304374m.

(11) Yang, Y.; Zhu, G.; Zhang, H.; Chen, J.; Zhong, X.; Lin, Z.-H.; Su, Y.; Bai, P.; Wen, X.; Wang, Z. L. Triboelectric Nanogenerator for Harvesting Wind Energy and as Self-Powered Wind Vector Sensor System. *ACS Nano* **2013**, *7* (10), 9461–9468. https://doi.org/10.1021/nn4043157.

(12) Wang, S.; Mu, X.; Wang, X.; Gu, A. Y.; Wang, Z. L.; Yang, Y. Elasto-Aerodynamics-Driven Triboelectric Nanogenerator for Scavenging Air-Flow Energy. *ACS Nano* **2015**, *9* (10), 9554–9563. https://doi.org/10.1021/acsnano.5b04396.

(13) Lin, L.; Hu, Y.; Xu, C.; Zhang, Y.; Zhang, R.; Wen, X.; Lin Wang, Z. Transparent Flexible Nanogenerator as Self-Powered Sensor for Transportation Monitoring. *Nano Energy* **2013**, *2* (1), 75–81. https://doi.org/10.1016/j.nanoen.2012.07.019.

(14) Bian, Y.; Jiang, T.; Xiao, T.; Gong, W.; Cao, X.; Wang, Z.; Wang, Z. L. Triboelectric Nanogenerator Tree for Harvesting Wind Energy and Illuminating in Subway Tunnel. *Adv. Mater. Technol.* **2018**, *3* (3), 1700317. https://doi.org/10.1002/admt.201700317.

(15) Hou, T.-C.; Yang, Y.; Zhang, H.; Chen, J.; Chen, L.-J.; Lin Wang, Z. Triboelectric Nanogenerator Built inside Shoe Insole for Harvesting Walking Energy. *Nano Energy* **2013**, *2* (5), 856–862. https://doi.org/10.1016/j.nanoen.2013.03.001.

(16) Yu, Y.; Li, Z.; Wang, Y.; Gong, S.; Wang, X. Sequential Infiltration Synthesis of Doped Polymer Films with Tunable Electrical Properties for Efficient Triboelectric Nanogenerator Development. *Adv. Mater.* **2015**, *27* (33), 4938–4944. https://doi.org/10.1002/adma.201502546.

(17) Kornbluh, R. D.; Pelrine, R.; Prahlad, H.; Wong-Foy, A.; McCoy, B.; Kim, S.; Eckerle, J.; Low, T. From Boots to Buoys: Promises and Challenges of Dielectric Elastomer Energy Harvesting. In *Electroactive Polymer Actuators and Devices (EAPAD) 2011*; International Society for Optics and Photonics, 2011; Vol. 7976, p 797605. https://doi.org/10.1117/12.882367.
(18) Ryu, H.; Lee, J.-H.; Kim, T.-Y.; Khan, U.; Lee, J. H.; Kwak, S. S.; Yoon, H.-J.; Kim, S.-W. High-Performance Triboelectric Nanogenerators Based on Solid Polymer Electrolytes with Asymmetric Pairing of Ions. *Adv. Energy Mater.* **2017**, *7* (17), 1700289. https://doi.org/10.1002/aenm.201700289.
(19) Chowdhury, A. R. Organic-Inorganic Hybrid Materials for Piezoelectric/Triboelectric Nanogenerator. M.S., The University of Texas Rio Grande Valley, United States -- Texas, 2020.
(20) Chowdhury, A. R.; Jaksik, J.; Hussain, I.; Tran, P.; Danti, S.; Uddin, M. J. Surface-Modified Nanostructured Piezoelectric Device as a Cost-Effective Transducer for Energy and Biomedicine. *Energy Technol.* **2019**, *7* (5), 1800767. https://doi.org/10.1002/ente.201800767.
(21) Chowdhury, A. R.; Jaksik, J.; Hussain, I.; Longoria, R.; Faruque, O.; Cesano, F.; Scarano, D.; Parsons, J.; Uddin, M. J. Multicomponent Nanostructured Materials and Interfaces for Efficient Piezoelectricity. *Nano-Struct. Nano-Objects* **2019**, *17*, 148–184. https://doi.org/10.1016/j.nanoso.2018.12.002.
(22) Chowdhury, A. R.; Abdullah, A. M.; Hussain, I.; Lopez, J.; Cantu, D.; Gupta, S. K.; Mao, Y.; Danti, S.; Uddin, M. J. Lithium Doped Zinc Oxide Based Flexible Piezoelectric-Triboelectric Hybrid Nanogenerator. *Nano Energy* **2019**, *61*, 327–336. https://doi.org/10.1016/j.nanoen.2019.04.085.
(23) Du, W.; Han, X.; Lin, L.; Chen, M.; Li, X.; Pan, C.; Wang, Z. L. A Three Dimensional Multi-Layered Sliding Triboelectric Nanogenerator. *Adv. Energy Mater.* **2014**, *4* (11), 1301592. https://doi.org/10.1002/aenm.201301592.
(24) Fuh, Y. K.; Wang, B. S. Near Field Sequentially Electrospun Three-Dimensional Piezoelectric Fibers Arrays for Self-Powered Sensors of Human Gesture Recognition. *Nano Energy* **2016**, *30* (Supplement C), 677–683. https://doi.org/10.1016/j.nanoen.2016.10.061.
(25) Hassan, G.; Khan, F.; Hassan, A.; Ali, S.; Bae, J.; Lee, C. H. A Flat-Panel-Shaped Hybrid Piezo/Triboelectric Nanogenerator for Ambient Energy Harvesting. *Nanotechnology* **2017**, *28* (17), 175402. https://doi.org/10.1088/1361-6528/aa65c3.
(26) Wang, X.; Yang, B.; Liu, J.; Zhu, Y.; Yang, C.; He, Q. A Flexible Triboelectric-Piezoelectric Hybrid Nanogenerator Based on P(VDF-TrFE) Nanofibers and PDMS/MWCNT for Wearable Devices. *Sci. Rep.* **2016**, *6*, 36409. https://doi.org/10.1038/srep36409.
(27) Wei, X. Y.; Zhu, G.; Wang, Z. L. Surface-Charge Engineering for High-Performance Triboelectric Nanogenerator Based on Identical Electrification Materials. *Nano Energy* **2014**, *10*, 83–89. https://doi.org/10.1016/j.nanoen.2014.08.007.
(28) Zhang, H.; Lu, Y.; Ghaffarinejad, A.; Basset, P. Progressive Contact-Separate Triboelectric Nanogenerator Based on Conductive Polyurethane Foam Regulated with a Bennet Doubler Conditioning Circuit. *Nano Energy* **2018**, *51*, 10–18. https://doi.org/10.1016/j.nanoen.2018.06.038.
(29) Diaz, A. F.; Felix-Navarro, R. M. A Semi-Quantitative Tribo-Electric Series for Polymeric Materials: The Influence of Chemical Structure and Properties. *J. Electrost.* **2004**, *62* (4), 277–290. https://doi.org/10.1016/j.elstat.2004.05.005.
(30) Song, P.; Yang, G.; Lang, T.; Yong, K.-T. Nanogenerators for Wearable Bioelectronics and Biodevices. *J. Phys. Appl. Phys.* **2018**, *52* (2), 023002. https://doi.org/10.1088/1361-6463/aae44d.
(31) Yoon, H.-J.; Ryu, H.; Kim, S.-W. Sustainable Powering Triboelectric Nanogenerators: Approaches and the Path towards Efficient Use. *Nano Energy* **2018**, *51*, 270–285. https://doi.org/10.1016/j.nanoen.2018.06.075.
(32) Gulmine, J. V.; Janissek, P. R.; Heise, H. M.; Akcelrud, L. Polyethylene Characterization by FTIR. *Polym. Test.* **2002**, *21* (5), 557–563. https://doi.org/10.1016/S0142-9418(01)00124-6.
(33) Zbinden, R. Infrared Spectroscopy of High Polymers. **1964**.
(34) Haslam, J.; Willis, H. A. Identification and Analysis of Plastics. *Identif. Anal. Plast.* **19650000**, 483–483.
(35) Zou, Y.; Tan, P.; Shi, B.; Ouyang, H.; Jiang, D.; Liu, Z.; Li, H.; Yu, M.; Wang, C.; Qu, X.; Zhao, L.; Fan, Y.; Wang, Z. L.; Li, Z. A Bionic Stretchable Nanogenerator for Underwater Sensing and Energy Harvesting. *Nat. Commun.* **2019**, *10* (1), 2695. https://doi.org/10.1038/s41467-019-10433-4.
(36) Gu, L.; Cui, N.; Cheng, L.; Xu, Q.; Bai, S.; Yuan, M.; Wu, W.; Liu, J.; Zhao, Y.; Ma, F.; Qin, Y.; Wang, Z. L. Flexible Fiber Nanogenerator with 209 V Output Voltage Directly Powers a Light-Emitting Diode. *Nano Lett.* **2013**, *13* (1), 91–94. https://doi.org/10.1021/nl303539c.

(37) Abdullah, A. M.; Flores, A.; Chowdhury, A. R.; Li, J.; Mao, Y.; Uddin, M. J. Synthesis and Fabrication of Self-Sustainable Triboelectric Energy Case for Powering Smart Electronic Devices. *Nano Energy* **2020**, *73*, 104774. https://doi.org/10.1016/j.nanoen.2020.104774.
(38) Zou, H.; Zhang, Y.; Guo, L.; Wang, P.; He, X.; Dai, G.; Zheng, H.; Chen, C.; Wang, A. C.; Xu, C.; Wang, Z. L. Quantifying the Triboelectric Series. *Nat. Commun.* **2019**, *10* (1), 1427. https://doi.org/10.1038/s41467-019-09461-x.
(39) Zhu, Y.; Yang, B.; Liu, J.; Wang, X.; Wang, L.; Chen, X.; Yang, C. A Flexible and Biocompatible Triboelectric Nanogenerator with Tunable Internal Resistance for Powering Wearable Devices. *Sci. Rep.* **2016**, *6* (1), 22233. https://doi.org/10.1038/srep22233.
(40) Williams, M. W. Triboelectric Charging of Insulating Polymers–Some New Perspectives. *AIP Adv.* **2012**, *2* (1), 010701. https://doi.org/10.1063/1.3687233.

Polymer Based Triboelectric Nanogenerator for Cost-Effective Green Energy Generation and Implementation of Surface-Charge Engineering

A cost-effective vertical contact separation mode triboelectric nanogenerator of high output has been designed and fabricated that scavenges energy from human footsteps and vehicle motion. The device has been tested considering real-world scenarios and has been finely tuned by testing variable impact distance, load frequency, and triboelectric airgap. The device has been further enhanced by surface-charge engineering that resulted in higher gain of power.